Individual Air-Borne Particle Mass Measurement Using High-Frequency Micromechanical Resonators

Arash Hajjam, *Student Member, IEEE*, James C. Wilson, and Siavash Pourkamali, *Member, IEEE*

***Abstract*—This work demonstrates mass measurement of individual submicron air-borne particles using resonant micromechanical nano-balances. Thermally actuated high-frequency single crystalline silicon resonators fabricated using a single mask process have been used as mass sensors. Mass sensitivity of the resonators have been characterized using artificially generated airborne particles of known size and composition. Mass sensitivities as high as 1.6 kHz/pg have been demonstrated for devices with resonant frequencies in the tens of MHz range. The measured mass sensitivities are in good agreement with the calculated values based on the resonator physical dimensions. Due to the high mass sensitivities, the shift in the resonator frequencies caused by individual particles as small as ∼200 nm in diameter is distinguishable. Counting and individual mass measurement of single arbitrary particles in air samples from a cleanroom have also been demonstrated. The results in this work present the possibility of implementation of low-cost and small-size instruments for airborne particle mass and size distribution analysis in highly controlled environments (e.g., for cleanroom classification) or for environmental applications.**

***Index Terms*—Air-borne particle, mass sensor, microelectromechanical systems (MEMS), particle sensor, piezoresistive readout, resonator, thermal actuation.**

I. Introduction

MEASUREMENT of concentration and size distribution of air-borne micro/nanoscale particles is of great interest to environmental scientists. This is mainly due to the high influence of air-borne particles on air quality and its effect on human health [1], [2], radiation balance of the earth (climate change) [3], and stratospheric ozone depletion [4]. Furthermore, monitoring of particle counts in highly controlled environments is an essential requirement for cleanrooms, clean benches, filter facilities in operating rooms, filling facilities in the pharmaceutical industry and filter efficiency test instruments.

Optical detection is the most common method used for detection, counting, and size measurement of micro/nanoscale air-borne particles. In the most basic version of optical particle sensors, particles are detected by a photodetector as they pass through the path of a laser beam. Optical measurement techniques of this kind do not always provide the required resolution and are limited to the light wavelength in terms of the minimum detectable particle size. They also need the integration of several optical components which make the overall system complex, costly, and bulky [5]–[7].

Resonant mass sensors such as Quartz Crystal Microbalance (QCM) [8], Surface Acoustic Wave (SAW) [9]–[12], and Film Bulk Acoustic resonators (FBAR) [13] have been used as alternatives to the optical techniques for particle sensing applications. Such devices can quantify the cumulative mass of air-borne particles deposited on their surfaces as a shift in their resonant frequency. However, they cannot provide the particle count and size distribution data which would require measurement of the mass of individual particles. In addition, in most cases they do not have the desired sensitivity.

Similar to the conventional resonant mass sensors, MEMS resonant mass sensors operate on the basis of the frequency shift caused by the added mass. The miniaturized MEMS resonators can be batch fabricated as individual devices or arrays at a very low cost [14], [15] and due to their much smaller size, they can provide orders of magnitude higher mass sensitivity and resolution compared to bulky quartz [16]–[18] and SAW [10], [19], [20] resonators or even FBARs [13]. Such devices also enable measurement of mass (and potentially size) of individual air-borne particles and therefore statistical distributions of such.

Most of the MEMS resonators used for sensory applications utilize piezoelectric [14] or electrostatic (capacitive) [21]–[23] electromechanical transduction. In case of air-gap capacitive resonators, extreme vulnerability of the air-gaps to contaminants or particulates makes it practically impossible to use them as particulate mass sensors. Moreover, small actuation forces of electrostatic actuators necessitate deep submicron transduction gaps leading to fabrication challenges, power handling limitations, and excessive squeezed film damping when operating in air. Piezoelectric microresonators, on the other hand, require deposition of piezoelectric and metal thin films generally resulting in lower quality factors, as well as frequency inaccuracy and quality control issues. In addition, it is very hard (if not impossible) to have a uniform mass sensitivity all over their sensing surface. This is due to the fact that such devices generally operate in their bulk resonant modes resulting in different vibration amplitudes and therefore different effective resonator mass at different locations of the structure. Uniform mass sensitivity is a necessity when targeting mass measurement of individual particles.

Manuscript received January 05, 2011; revised February 27, 2011; accepted April 14, 2011. Date of publication April 25, 2011; date of current version October 26, 2011. The associate editor coordinating the review of this paper and approving it for publication was Prof. Weileun Feng.

A. Hajjam and S. Pourkamali are with the Department of Electrical and Computer Engineering, University of Denver, Denver, CO 80208 USA (e-mail: ahajjam@du.edu; spourkam@du.edu).

J. C. Wilson is with the Department of Materials and Mechanical Engineering, University of Denver, Denver, CO 80208 USA (e-mail: jwilson@du.edu).

Color versions of one or more of the figures in this paper are available online at http://ieeexplore.ieee.org.

Digital Object Identifier 10.1109/JSEN.2011.2147301

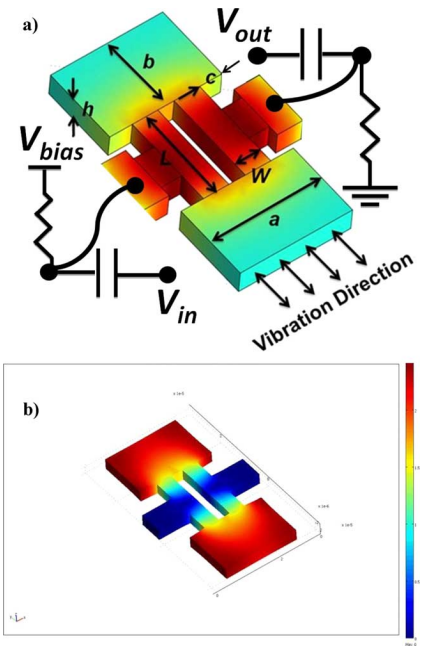

Fig. 1. (a) Schematic view of the utilized thermally actuated resonant sensors showing the qualitative distribution of AC temperature fluctuation amplitude (red being the maximum and blue the minimum). The electrical connections required for one-port operation of the resonator are also shown. (b) COMSOL eigen frequency analysis results showing the fundamental in-plane resonance mode shape for an IBAR.

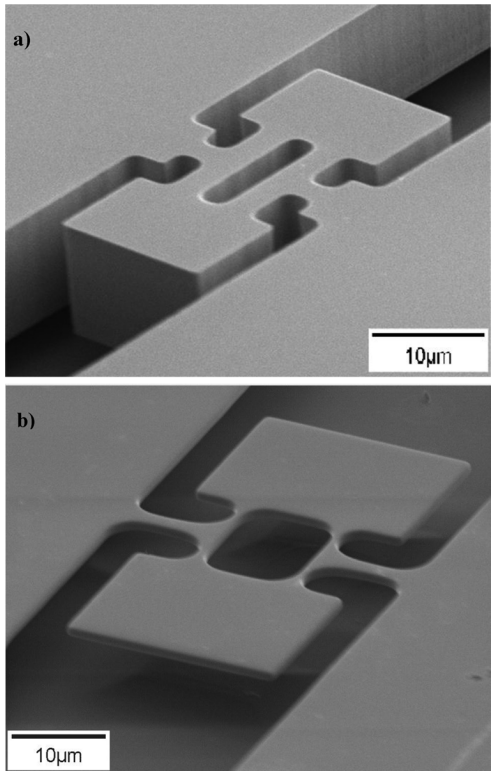

Fig. 2. SEM views of two of the fabricated IBARs. (a) A 61 MHz, 15 μm thick resonator. (b) A fabricated 20.5 MHz, 2.7 μm thick resonator. Both resonators were etched using DRIE (ICP + Bosch process).

Electrothermal actuators are extremely simple to implement requiring only a heating resistance. They are also very suitable for actuation of in-plane translational resonance modes, providing uniform mass sensitivity over a big portion of the resonator surface area [24]. Thermally actuated micromechanical resonators have shown suitability and robustness for airborne particle cumulative mass measurements [15], [25], [26]. This work presents smaller and higher frequency versions of such devices capable of detection and measurement of single submicron particles.

II. Resonator Description and Fabrication

The resonators utilized in this work are referred to as I-Shaped Bulk Acoustic Resonators (IBARs; also known as dog-bone resonators) [27], [28]. The schematic view of a thermally actuated IBAR is shown in Fig. 1(a). Such devices are very suitable for thermal actuation as they can easily be actuated by passing a fluctuating electrical current between the two pads on their two sides. This results in an AC ohmic loss component in the current path. Due to their higher resistance, most of the ohmic loss occurs in the thin pillars located in the middle of the structure. The AC force generated in the pillars as a result of the fluctuating temperature and therefore alternating thermal stress in the pillars, can actuate the resonator in its in-plane resonant mode. Fig. 1(a) shows the qualitative distribution of AC temperature fluctuation amplitude. The electrical connections and components required for isolation of the AC actuation current from the DC bias current required for operation of the resonator [28] are also shown in Fig. 1(a). Fig. 1(b) shows the in-plane extensional resonant mode of the resonators. In this mode, the masses on the two ends of the pillars vibrate back and forth in opposite directions. At resonance, the resistance of the pillars will be modulated by the resulting alternating mechanical stress due to the piezoresistive effect that results in a detectable small signal motional current in the device.

The standard single mask SOI MEMS process was used for fabrication of the resonators. This process includes carving the single crystalline silicon structures into the SOI device layer (by deep reactive ion etching) followed by removing the underlying buried oxide layer (BOX) in hydrofluoric acid (HF) [25]. The resonators were fabricated on two different low resistivity SOI substrates: 1) a P-type SOI substrate with device layer thickness of 15 μm and buried oxide layer (BOX) thickness of 5 μm and 2) an N-type SOI substrate with both device layer and BOX thickness of 5 μm, respectively.

Fig. 2 shows the SEM view of two of the fabricated IBARs which were used in the experiments. For the bottom device, the actuator beams were thinned down in order to minimize resonator power consumption. This was done by performing a number of consecutive thermal oxidation and oxide removal steps after the devices were released. At the same time, the resonator thicknesses were also reduced.

Due to the nearly rigid body of the moving plates of the resonators, their deformation in the in-plane resonance mode is negligible. Therefore, the whole plate vibrates with relatively uniform vibration amplitude. As a result, the effect of similar particles added to different locations on the plate, on the overall resonance frequency of the structure will be the same (uniformity of mass sensitivity) [24].

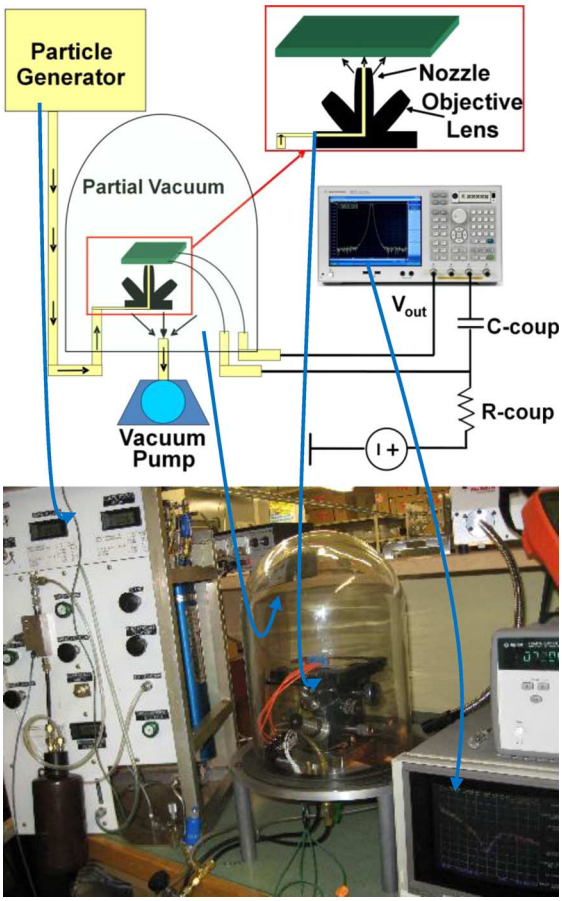

Fig. 3. Schematic view and camera picture of the setup used to characterize the resonator mass sensitivities.

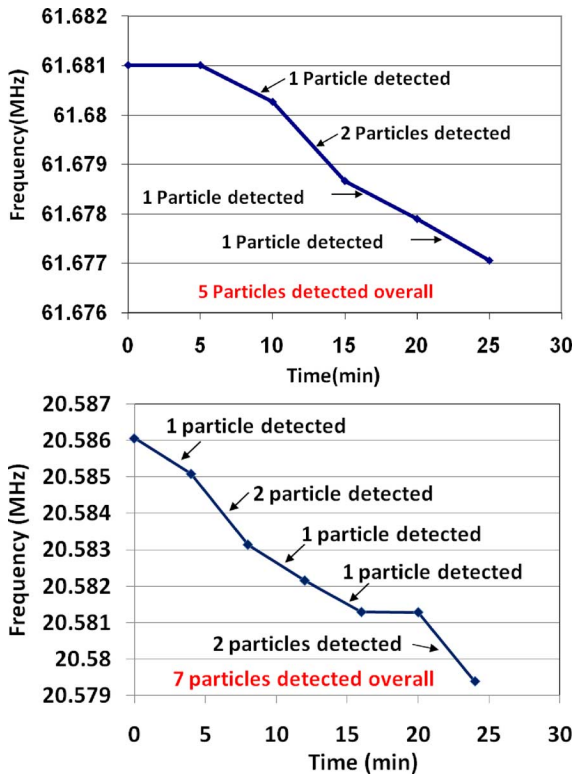

Fig. 4. The top graph shows the measured resonance frequency for the 61 MHz resonator of Fig. 2(a) as a function of the overall exposure time showing an overall frequency shift of ~ 4 kHz (65 ppm). The figure shows four consecutive reduction steps with one of the steps having a slope twice the rest showing that two particles have been deposited during that specific interval (10–15 min). The bottom figure is showing the change in the measured resonance frequency versus time for the 20 MHz resonator of Fig. 2(b) showing an overall frequency shift of ~ 6.7 kHz (325 ppm). Here, there are five frequency reduction steps, of which two have a slope twice that of the rest which again shows that two particles have been deposited on the device during that period. In conclusion, five particles and seven particles have overall been deposited on the 61 and 20 MHz resonator, respectively.

III. Resonator Mass Sensitivity Characterization

In order to characterize mass sensitivity of the fabricated resonators, the silicon chip containing the devices was placed on a printed circuit board (PCB) containing the required resistors and capacitors to apply DC bias and AC actuation currents to the resonators. The value of the bias resistors and isolation capacitors were 100 Ω and 0.1 μF, respectively.

Connections to the resonators were provided by wedge-bonded aluminum wires. The PCB was then embedded in a custom made setup comprised of a sealed vacuum chamber, an aerosol particle generator, and an alignment apparatus. The schematic diagram and camera picture of the test setup is shown in Fig. 3.

In the aerosol particle generator, a flow of methylene blue solution in ethanol generated by a micro syringe pump is first atomized in an air-blast nebulizer by a nitrogen flow which produces a mist of droplets [15].

The droplets are passed through a Kr-85 bipolar diffusion charger that neutralizes most of the charge left on the droplets as a result of atomization and establishes a charge distribution close to Boltzman distribution for the droplets (mostly neutral, some $\pm 1q$, less $\pm 2q$, etc., where q is the charge of a single electron). In the meanwhile, the solvent in the droplets is evaporated and the dried polydisperse aerosol is injected into a differential mobility analyzer that separates the particles using an electrostatic field (based on their mass and electric charge) allowing only particles with specific diameter and charge to pass through it. The electric field and flows were regulated to permit selection of particles with a diameter close to 1 μm [25]. Particles coming out of the particle generator are then directed into the low pressure (50–100 Torr) chamber by the partial vacuum generated by a vacuum pump connected to the inlet of the bell-jar chamber.

In the chamber, the PCB is horizontally placed on a micropositioning alignment apparatus. The alignment apparatus consists of a microscope with one of its objective lenses replaced by the nozzle carrying the flow of particles from the generator. Once the microscope lens is aligned directly on top of the specific resonator to be characterized, the head is turned so that the nozzle points directly towards the device under test. Therefore, particles coming out of the particle generator are deposited on the resonator under test. Resonators with different dimensions were exposed to the flow of particles for several consecutive intervals of a few minutes each. After each interval, the resonator characteristics were measured and recorded.

Fig. 4 shows the resonant frequency of the 61 and 20 MHz resonators of Fig. 2 versus the overall exposure time after each

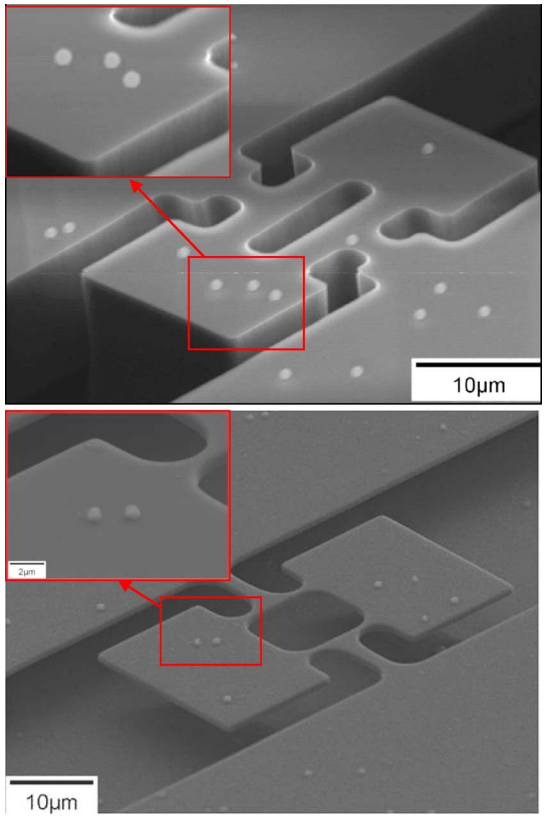

Fig. 5. SEM view of the resonators of Fig. 2 after exposure to aerosol particles for 25 and 24 minutes, respectively; showing five and seven spherical particles deposited on their two sensing plates.

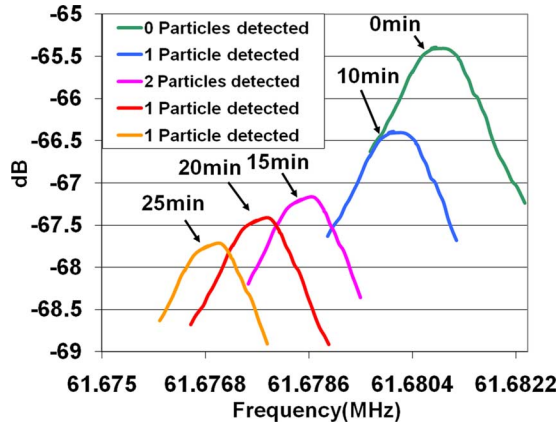

Fig. 6. Measured frequency responses for the 61 MHz resonator of Fig. 2(a), while biased at a constant current after different exposure intervals.

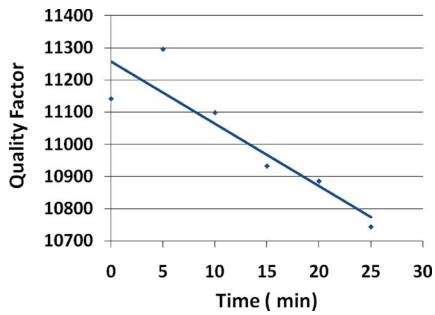

Fig. 7. Measured quality factor versus overall exposure time to aerosol particles for the to 61 MHz resonator in Fig. 2(a).

exposure step. It is clear that reduction of the resonant frequency of the resonator is quantized and occurs in steps that are multiples of ~ 800 Hz for the 60 MHz and ~ 900 Hz for the 20 MHz resonator. This makes the effect of every single particle on the resonance frequency distinguishable.

Fig. 5 shows the SEM view of the resonators of Fig. 2 after 25 and 24 min of exposure showing exactly five and seven spherical particles of $\sim 1\ \mu$m diameter deposited on their two sensing plates. This is in complete agreement with the step by step frequency shifts shown in Fig. 4. In case of the first resonator, the particle on the thermal actuator beam has negligible effect on the resonant frequency since the vibration amplitude at that location is very small compared to the plates. Particles sitting on different locations of the thermal actuator beams will have different effects on the resonance frequency of the structure (due to different vibration amplitudes and therefore different effective stiffness and effective resonator mass at different locations). However, since the overall surface area of the thermal actuator beams are typically much smaller than that of the plates, the resulting error could be negligible. To further increase the precision of measurements one can add a shadowing stationary surface covering the thermal actuator beams.

Fig. 6 shows different measured frequency response plots for the 61 MHz resonator of Fig. 2 during particle deposition. As shown in Fig. 7, the resonator quality factor is slightly degraded as more particles are deposited on it and that is the reason why the peak signal level decreases over time in Fig. 6.

The mass sensitivity of the resonators can be theoretically calculated based on the resonant frequency and effective mass of the resonator as follows:

$$f = \frac{1}{2\pi}\sqrt{\frac{k}{m}} \Rightarrow \frac{\partial f}{\partial m} = -\frac{f}{2m} \tag{1}$$

where k, m, and f are the effective stiffness, effective mass and resonant frequency of the resonator, respectively.

Knowing the dimensions and therefore the effective mass of the resonators, the overall mass of the deposited particles (δm) were estimated from the measured frequency shifts (δf).

The overall mass of the particles was also independently calculated based on the number of the deposited particles given by SEM inspections of Fig. 5.

Table I summarizes the measurement results for the tested resonators and compares the experimental frequency shift caused by the added mass of the particles (~0.65 pg per particle) with the expected frequency shift according to the mass of the resonator and (1), showing a good agreement between the two.

Resonator mass sensitivities are in the 1.1–1.7 kHz/pg range. As expected, devices with higher frequency and smaller size have higher sensitivities.

The demonstrated mass sensitivities are orders of magnitude higher than the reported values for conventional quartz [16]–[18], [29], [30], SAW [10], [19], [29], and even FBARs [13], [30] due to their much smaller sizes. Table II shows the comparison between the mass surface density sensitivity and

TABLE I
SUMMARY OF MEASUREMENT RESULTS OBTAINED FROM THE TWO RESONATORS IN FIG. 2 AND COMPARISON OF THE MEASURED MASS SENSITIVITY WITH THE THEORETICALLY PREDICTED MASS SENSITIVITY

Resonator Dimensions (μm)		Q factor	Freq (MHz)	Time (min)	Freq. Shift (Hz)	No. of particles detected	Overall Mass from freq. shift (pg)	Overall Mass from Microscope count (pg)	Calculated Sensitivity (kHz/pg)	Measured Sensitivity (kHz/pg)
a-b-c	L-W-h									
22-15.4-4.4	17.6-5-15	11140	61.68101	0	-	-	3.43	3.22	1.152	1.228
		11300	61.68101	5	0	0				
		11100	61.680268	10	-742	1				
		10930	61.678668	15	-1600	2				
		10890	61.677896	20	-771	1				
		10740	61.677055	25	-842	1				
30-19.7-7	15-0.8-2.7	5120	20.58606	0	-	-	4.877	4.508	1.369	1.481
		5010	20.585085	4	-975	1				
		4960	20.58314	8	-1945	2				
		4730	20.582151	12	-989	1				
		4600	20.581286	16	-865	1				
		4610	20.581279	20	-7	0				
		4350	20.579381	24	-1898	2				
29.9-20-7	14-1.9-2.7	4595	26.962981	0	-	-	2.283	2.576	1.727	1.593
		4580	26.962973	4	-8	0				
		4410	26.962049	8	-924	1				
		4340	26.960979	12	-1070	1				
		4290	26.960972	16	-7	0				
		4165	26.959944	20	-1028	1				
		4025	26.958886	24	-1058	1				

TABLE II
COMPARISON OF THE MASS SURFACE DENSITY SENSITIVITY AND ABSOLUTE MASS SENSITIVITY AS WELL AS RESOLUTION OF THE THERMALLY ACTUATED IBARS WITH THAT OF DIFFERENT TECHNOLOGIES SUCH AS QCM, SAW, AND FBAR

Type of Sensor	Mass Surface Density Sensitivity / Mass Sensitivity	Mass Surface Density Resolution /Mass Resolution
QCM	$0.3-1.6\frac{Hz.cm^2}{ng}$ [29, 30] / $1\frac{Hz}{ng}$ [10]	$\sim 10\frac{ng}{cm^2}$ [29, 30] / $3000pg$ [10]
SAW	$15\frac{Hz.cm^2}{ng}$ [29] / $260\frac{Hz}{ng}$ [10]	$\sim 1\frac{ng}{cm^2}$ [29] / $0.3pg$ [10]
FBAR	$\sim 800\frac{Hz.cm^2}{ng}$ [13, 30]	$2.5\frac{ng}{cm^2}$ [30] / $1pg$ [13]
Piezoelectrically Actuated MEMS	$10\frac{Hz.cm^2}{ng}$ / $4\frac{kHz}{ng}$ [14]	$1\frac{\mu g}{cm^2}$ / $0.25pg$ [14]
Thermally Actuated MEMS	$15\frac{Hz.cm^2}{ng}$ / $1500\frac{kHz}{ng}$	$0.6\frac{ng}{cm^2}$ / $0.01pg$

absolute mass sensitivity as well as resolution for different technologies. The sensitivity that matters in this application is the absolute mass sensitivity, for which our device by far shows better sensitivity when compared to other technologies.

In our experimental setup, a minimum frequency shift of 10 Hz could easily be detected using the network analyzer. For resonator mass sensitivity of 1.6 kHz/pg, the experimental minimum detectable mass is approximately 7 fg.

However, this limit is much smaller than the limit imposed by the temperature induced frequency drift of the devices.

Assuming temperature uncertainty of 10 °C (which is typical in targeted environmental applications) and typical resonator temperature coefficient of frequency (TCF) of -40 ppm/°C [31] for uncompensated silicon resonators, the frequency of a 26 MHz resonator could shift by up to 10.5 kHz due to temperature. This limits the mass resolution to $\sim$ 6 pg. TCF as low as -0.05 ppm/°C has been achieved for compensated version of thermally actuated silicon resonators [31] reducing the temperature induced frequency inaccuracy of the same 26 MHz resonator to 13 Hz. This translates into a mass resolution of $\sim$ 9 fg, which is equivalent to a particle diameter of $\sim$ 180 nm.

Minimum detectable mass limits in the tens of picogram range [16], [29] for QCM and SAW resonators and in the picogram range [13], [30] for FBARs have been reported.

However, such estimates generally neglect the effect of temperature induced frequency uncertainties that typically make further increases of the minimum detectable limits.

IV. ARBITRARY AIR-BORNE PARTICLE MEASUREMENTS

After characterizing the resonator mass sensitivities using known particles, their performance in a real world application when exposed to arbitrary air-borne particles was investigated. In this experiment, the PCB was placed in the same low pressure chamber. An air inlet, internally connected to the particle deposition nozzle, was left open allowing the air from outside (internal cleanroom air along with the particles suspended in it) to be sucked into the chamber and deposited on the resonator under test. The tests were carried out in the cleanroom (a class 1000 standard) so that a smaller number of air-borne particles

TABLE III
SUMMARY OF MEASUREMENT RESULTS OBTAINED FROM THE RESONATORS EXPOSED TO THE FLOW OF AIR-BORNE PARTICLES IN A CLASS 1000 SOFTWALL CLEANROOM. THEORETICALLY PREDICTED MASS SENSITIVITY AS WELL AS THE SIZE DISTRIBUTION DATA FOR THE PARTICLES DEPOSITED ON EACH RESONATOR IS INCLUDED

Resonator Dimensions (μm)		Q factor	Freq. (MHz)	Time (sec)	Freq. Shift (Hz)	% of particles detected for different diameters (μm)							Δm Accumulative mass (pg)	S_{theory} (kHz/pg)
a-b	L-W-h					0.2 - 0.3	0.3 - 0.4	0.4 - 0.5	0.5 - 0.6	0.6 - 0.7	0.7 - 0.8	0.8 - 1		
29.5-22	10.5-2.9-3.2	3680	29.153	350	-4960	0	6.2	25	37.5	18.7	6.2	6.2	3.35	1.471
30.5-21	10.5-3.5-3.2	3930	27.271	440	-3905	7.1	14.2	28.5	21.4	14.2	7.1	7.1	2.84	1.387
28-20.5	9-3.5-3.2	3850	26.642	460	-4570	4.7	14.2	28.5	28.5	19	0	4.7	3.53	1.371
31-20.5	12-3-3.2	4520	24.828	420	-3720	5.5	11.1	50	16.6	11.1	0	5.5	2.91	1.273
31.5-21.5	12.4-3-3.2	3970	22.964	640	-4700	8.3	16.7	29.1	20.8	12.5	4.2	8.3	4.56	1.106
31.5-21.5	12-3-3.2	4100	21.959	440	-2940	7.1	21.4	35.7	28.6	7.1	7.1	7.1	2.89	1.058

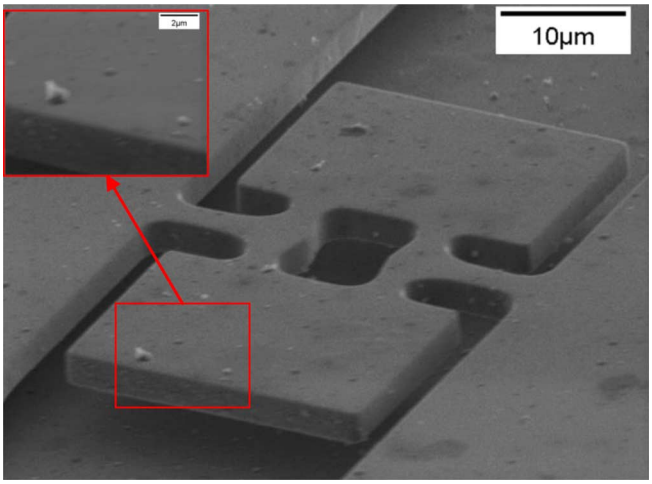

Fig. 8. SEM view of one of the thermally actuated IBAR resonators after being tested under exposure to aerosol particles in the cleanroom environment for a total time of 640 s.

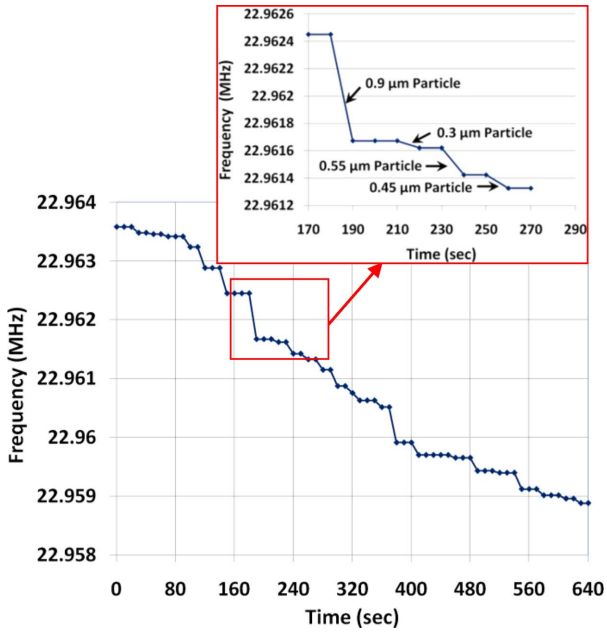

Fig. 9. Change in the measured resonance frequency for a 22.9 MHz 3.2 μm resonator as a function of the overall exposure time showing an overall frequency shift of ~ 4.7 kHz (205 ppm). Zoomed in view of the graph shows the amount of frequency shift during each interval allowing determination of the size of the deposited particle in each period.

would be deposited on the resonator. This would allow enough time between arrival of different particles making it possible to detect and measure the effect of each particle by having small exposure intervals. A valve was also connected to the air inlet to allow turning the particle flow on and off. With the inlet valve closed, under a constant bias current, the resonance frequency was recorded. The inlet valve was then opened exposing the resonator under test to the air flow and consequently the aerosol particles. The exposure was done in 10 s intervals and after each exposure the resonator parameters were measured and recorded. With such relatively short exposure interval, in some intervals there were no particles deposited on the resonator. Therefore, when there was an actual frequency shift in an interval, with a good approximation it could be assumed to be due to a single particle deposited on the surface of the device. It should be mentioned that using the current devices, particles smaller than 200 nm in diameter size could not be detected. Fig. 8 shows the SEM view of one of the tested resonators after it was exposed to the air-borne particles in the cleanroom for 640 s. Fig. 9 shows the measured resonance frequency as a function of the exposure time. It should be noted that the resonator quality factors are surprisingly robust to the deposited particles. After deposition of tens of particles of different sizes, no significant Q degradation was observed. This demonstrates their much higher robustness compared to capacitive resonators with extremely vulnerable air-gaps and multilayered thin-film piezoelectric resonators.

Based on the graph shown in Fig. 9 and also the shift in frequency at each step, the deposited mass during that period can easily be calculated. Assuming an approximate density of 3 $\mathrm{g/cm^3}$ for the particles, the approximate diameter of the deposited particles in each time period could also be estimated. Figs. 10 and 11 show the mass and diameter distribution of particles extracted from the measured frequency shifts for the 22.9 MHz resonator of Fig. 8.

Table III summarizes the measurement results for the different resonators tested in the cleanroom. The theoretical sensitivity is calculated based on the device dimensions of each device. Knowing the sensitivity, the total deposited mass which is also separately shown in the table can be derived.

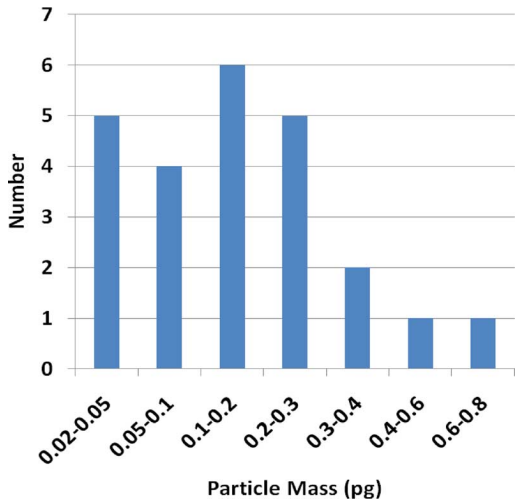

Fig. 10. Graph showing the mass distribution of particles deposited on the 22.9 MHz device shown in Fig. 8 based on measurement results shown in Fig. 9.

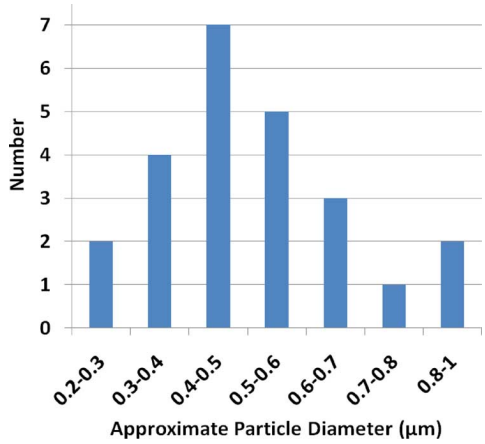

Fig. 11. Graph showing the size distribution of particles deposited on the 22.9 MHz device shown in Fig. 8. The density of the deposited particles was assumed to be 3 $\mathrm{g/cm^3}$.

The distributive percentage of particles with diameters in different ranges deposited on each device is also included in the table. The overall air volume that was sucked into the vacuum chamber was calculated to be 1.2 $\mathrm{ft^3}$. However also taking the ratio of the landing zone surface to the device surface area into account, the amount of air volume (that particles were collected from) actually being blown onto the device was $8 * 10^{-3}$ $\mathrm{ft^3}$. Cleanrooms are classified according to the number and size of particles permitted per volume of air. For a class 1000 of the US FED STD 209E standard, approximately 1000 particles per cubic foot with diameter ranges between 0.5 and 5 $\mu\mathrm{m}$ are permitted. Particle sizes less than 0.5 $\mu\mathrm{m}$ in diameter size are non-applicable combinations for this class. Taking into account the amount of air volume which the particles in the experiments were collected from, there should be roughly ten particles in that diameter range collected.

Based on this, it was demonstrated that the particle concentration distribution in our cleanroom closely matches that of the class 1000 standard.

V. Conclusion and Future Work

Thermally actuated single crystalline silicon in-plane high-frequency resonators with piezoresistive readout were fabricated and utilized as particulate mass sensors. Devices with frequencies up to 61 MHz were used to measure the mass of individual artificially generated air-borne particles. Mass sensitivities as high as 1.6 kHz/pg were measured for the resonators. Comparison of the measured and calculated mass sensitivities shows a good agreement between the two.

Mass measurement of individual arbitrary airborne particles in the cleanroom air sample was carried out using the same resonators. Due to the high mass sensitivity of the devices, individual particles as small as 200 nm in diameter deposited during each period of time could be distinguished. By counting and sizing the number of collected particles in an air volume, the cleanroom was classified. Furthermore, orders of magnitude higher mass sensitivities are achievable by further reducing the thickness and horizontal dimensions of the resonators.

Future work includes further design optimization and miniaturization of the resonator dimensions to achieve higher mass sensitivity. Arrays of devices with different size could be batch fabricated enabling the detection of particles with a variety of size distributions using different devices. Other future work involves the integration of piezoresistive impact sensing mechanism in the structure of sensor enabling us to measure the impact force (kinetic energy) of the individual particles along with their mass. Combining the mass and energy measurements for individual particles permits the collision velocity to be determined, which leads to the determination of particle size in situations where the velocity is size dependent.

References

[1] Z. Sun, Z. Huang, and J. S. Wang, "Studies on the size distribution, number and mass emission factors of candle particles characterized by modes of burning," *J. Aerosol Sci.*, vol. 37, pp. 1484–96, 2006.

[2] U. Poschl, "Atmospheric aerosols: Composition, transformation, climate and health effects," *J. Atmospheric Chem. Sci.*, vol. 44, pp. 7520–40, Nov. 2005.

[3] V. Ramanathan, P. J. Crutzen, J. Kiehl, and D. Rosenfeld, "Aerosols, climate, and the hydrological cycle," *J. Science*, vol. 294, no. 5549, pp. 2119–24.

[4] P. A. Newman and J. A. Pyle, "Polar stratospheric ozone: Past and future, in scientific assessment of ozone depletion," World Meteorological Organization, Geneva, Switzerland, Global Ozone Res. Monitoring Project- Rep. No. 47, 2003, .

[5] D. S. Covert, J. Heintzenberg, and H. Hansson, "Electro-optical detection of external mixtures in aerosols," *J. Aerosol Sci. Technol.*, vol. 12, no. 2, pp. 446–56, 1990.

[6] M. V. Panchenko, M. A. Sviridenkov, S. A. Terpugova, and V. S. Kozlov, "Active spectral nephelometry as a method for the study of submicron atmospheric aerosols," *J. Remote. Sensing*, vol. 29, no. 9, pp. 2567–2583, 2008.

[7] K. M. Davitt *et al.*, "A compact aerosol sensor and spectroscopic sorting with UV LEDs," in *Proc. Optically Based Biol. Chem. Detection for Defense Conf.*, 2006, pp. 63980–989.

[8] D. Liang, W. P. Shih, C. S. Chen, and C. Dai, "A miniature system for separating aerosol particles and measuring mass concentrations," *J. Sensor*, vol. 10, pp. 3641–3654, Apr. 2010.

[9] W. D. Bowers, R. L. Chuan, and T. M. Duong, "A 200 MHz surface acoustic wave resonator mass microbalance," *Rev. Sci. Instrum.*, vol. 62, no. 6, pp. 1624–1629, 1991.

[10] W. D. Bowers and R. L. Chuan, "Surface acoustic-wave piezoelectric crystal aerosol mass microbalance," *Rev. Sci. Instrum.*, vol. 60, pp. 1297–1302, 1991.

[11] S. M. Stanley, G. McHale, M. Newton, C. J. Percival, and R. Evans, "An EP-SAW for measurements of particle matter in ambient air," *J. Nondestructive Testing and Evaluation*, vol. 20, no. 1, pp. 3–7, 2005.
[12] P. A. Baron and K. Willeke, *Aerosol Measurement, Principles, Techniques and Applications*, 2nd ed. New York: Wiley.
[13] J. P. Black, A. Elium, R. M. White, M. G. Apte, L. A. Gundel, and R. Cambie, "MEMS-enabled miniaturized particulate matter monitor employing 1.6 GHz aluminum nitride thin-film bulk acoustic wave resonator (FBAR) and thermophoretic precipitator," in *Proc. IEEE Ultrasonics Symp.*, 2007, pp. 476–480.
[14] B. Harrington, A. Hajjam, J. C. Wilson, S. Pourkamali, and R. Abdolvand, "Thin-film piezoelectric-on-silicon particle mass sensors," in *Proc. IEEE IFCS10*, 2010, pp. 238–241.
[15] A. Hajjam, J. C. Wilson, A. Rahafrooz, and S. Pourkamali, "Fabrication and characterization of thermally actuated micromechanical resonators for airborne particle mass sensing: II. Device fabrication and characterization," *J. Micromech. Microeng.*, vol. 20, p. 12501, Dec. 2010.
[16] L. Rodriguez-Pardo *et al.*, "Sensitivity, noise, and resolution in QCM sensors in liquid media," *IEEE J. Sensors*, vol. 5, no. 6, pp. 1251–58, Dec. 2005.
[17] D. C. Woods and R. L. Chuan, "Aerosol characterization with a quartz crystal microbalance cascade impactor," in *Proc. Adv. Particulate Sampling and Meas.*, 1979, vol. 22, pp. 1639–45.
[18] J. Leskinen *et al.*, "Diffusion based nanoparticle monitor using QCM-technology," in *Proc. Eur. Aerosol Conf.*, 2009, pp. 247–50.
[19] T. M. Bhide *et al.*, "Shear horizontal surface acoustic wave sensor platform development for chemical and biological detection," *J. Anal. Chem.*, vol. 73, pp. 5937–44, 2001.
[20] E. Berkenpas *et al.*, "Pure shear horizontal SAW biosensor on langasite," *IEEE Trans. Ultrason., Ferroelectr., Freq. Control*, vol. 51, pp. 1404–11, 2004.
[21] Z. Hao, R. Abdolvand, and F. Ayazi, "A high-Q length-extensional bulk-mode mass sensor with annexed sensing platforms," in *Proc. IEEE MEMS'06*, 2006, pp. 598–601.
[22] S. Kim, T. Ono, and M. Esashi, "Capacitive resonant mass sensor with frequency demodulation detection based on resonant circuit," *Appl. Phys. Lett.*, vol. 88, p. 053116, 2006.
[23] A. Rahafrooz and S. Pourkamali, "Detection of sub-ppm traces of aqueous heavy-metal ions using micro-electro-mechanical beam resonators," *J. Micromech. Microeng.*, vol. 19, no. 115003, Nov. 2009.
[24] A. Hajjam, J. C. Wilson, A. Rahafrooz, and S. Pourkamali, "Detection and mass measurement of individual air-borne particles using high frequency micromechanical resonators," in *Proc. IEEE Sensors*, Nov. 2010, pp. 2000–2004.
[25] A. Hajjam, J. C. Wilson, A. Rahafrooz, and S. Pourkamali, "Fabrication and characterization of resonant aerosol particle mass sensors," in *Proc. IEEE MEMS*, Dec. 2010, pp. 862–866.
[26] A. Hajjam, A. Rahafrooz, J. C. Wilson, and S. Pourkamali, "Thermally actuated MEMS resonant sensors for mass measurement of micro/nanoscale aerosol particles," in *Proc. IEEE Sensors*, New Zealand, Oct. 2009, pp. 707–710.
[27] G. K. Ho, K. Sundaresan, S. Pourkamali, and F. Ayazi, "Micromechanical IBARs: Tunable high-Q resonators for temperature-compensated reference oscillators," *J. Microelectromech. Syst.*, vol. 19, no. 3, pp. 503–515, Jun. 2010.
[28] A. Rahafrooz, A. Hajjam, B. Tousifar, and S. Pourkamali, "Thermal actuation, a suitable mechanism for high-frequency electromechanical resonators," in *Proc. 23rd IEEE MEMS*, Hong Kong, China, Jan. 2010, pp. 200–203.
[29] M. Ward and D. Buttry, "*In situ* interfacial mass detection with piezoelectric transducers," *J. Science*, vol. 249, pp. 1000–6, 1989.
[30] J. Weber *et al.*, "Shear mode FBARs as highly sensitive liquid biosensors," *J. Sens. Actuators*, vol. 128, pp. 84–8, 2006.
[31] A. Hajjam, A. Rahafrooz, and S. Pourkamali, "Sub-100 $\mathrm{ppb}/^{\circ}\mathrm{C}$ temperature stability in thermally actuated high frequency silicon resonators via degenerate phosphorous doping and bias current optimization," in *Proc. IEEE Int. Electron Device Meeting (IEDM)*, 2010, pp. 7.5.1–7.5.4.

Arash Hajjam (S'09) was born in Tehran, Iran. He received the B.S. degree in electrical engineering from the University of Tehran, Tehran, Iran, in 2005 and the M.S. degree in bio-electrical engineering from Iran University of Science and Technology, Tehran, in 2008. He is currently working towards the Ph.D. degree at the Department of Electrical and Computer Engineering, University of Denver, Denver, CO. His research interests are mainly related to microelectromechanical system frequency references and resonant sensors.

Mr. Hajjam is a 2009 recipient of the Best Teaching Assistant Award at the University of Denver, School of Engineering and Computer Science, the Best Student Paper Award at the ISCEE 2004 Electrical Engineering Conference, and the Professional Engineering (PE) License in the state of Colorado.

James C. Wilson received the Ph.D. degree in mechanical engineering from the University of Minnesota, Minneapolis, in 1977.

He is John Evans Professor of Mechanical and Materials Engineering at the University of Denver. His aerosol research group develops and uses instruments and sampling inlets to characterize airborne particles. It has operated instruments and inlets on NASA, NOAA, NSF, and U.K. Met Office aircraft from 72 S to 90 N and from sea level to 22 km altitude. They study air quality, the impact of volcanic eruptions, the role of particles in ozone depletion, new particle formation, and aerosol-cloud interactions.

Siavash Pourkamali (S'02–M'06) received the B.S. degree in electrical engineering from Sharif University of Technology, Tehran, Iran, in 2001, and the M.S. and Ph.D. degrees in electrical engineering from Georgia Institute of Technology, Atlanta, in 2004 and 2006, respectively.

He is currently an Assistant Professor at the Department of Electrical and Computer Engineering, University of Denver. His main research interests are in the areas of integrated silicon-based MEMS and microsystems, micromachining technologies, RF MEMS resonators and filters, and nanomechanical resonant sensors. He holds several issued patents and pending patent applications in the areas of silicon micro/nanomechanical resonators and filters and nanofabrication technologies, some of which have been licensed to major players in the semiconductor industry.

Dr. Pourkamali is a recipient of the 2011 NSF CAREER Award, the 2008 University of Denver Best Junior Scholar Award, and the 2006 Georgia Tech Electrical and Computer Engineering Research Excellence Award. He is also a silver medal winner in the 29th International Chemistry Olympiad (ICHO), 1997.